Dynamic Metabolic Modeling for a MAB Bioprocess

Jianying Gao,[†] Volker M. Gorenflo,[†] Jeno M. Scharer,[‡] and Hector M. Budman*[,‡]

Sanofi Pasteur Limited, Toronto, ON, Canada M2R 3T4, and Department of Chemical Engineering, University of Waterloo, Waterloo, ON, Canada N2L 3G1

Production of monoclonal antibodies (MAb) for diagnostic or therapeutic applications has become an important task in the pharmaceutical industry. The efficiency of high-density reactor systems can be potentially increased by model-based design and control strategies. Therefore, a reliable kinetic model for cell metabolism is required. A systematic procedure based on metabolic modeling is used to model nutrient uptake and key product formation in a MAb bioprocess during both the growth and post-growth phases. The approach combines the key advantages of stoichiometric and kinetic models into a complete metabolic network while integrating the regulation and control of cellular activity. This modeling procedure can be easily applied to any cell line during both the cell growth and post-growth phases. Quadratic programming (QP) has been identified as a suitable method to solve the underdetermined constrained problem related to model parameter identification. The approach is illustrated for the case of murine hybridoma cells cultivated in stirred spinners.

Introduction

Mammalian cell culture represents a major platform for the production of a number of high-value biopharmaceuticals, including enzymes, monoclonal antibodies (MAb), viral vaccines, hormones, and immuno-regulators. The products often require highly specialized culture conditions and are susceptible to either reduced productivity or significant cell death as a result of slight changes in culture conditions. The systematic integration of cell physiology into a coherent, predictive model, which can be used for simulation, optimization, and control, is expected to contribute to increased productivity and product quality.

Since earlier modeling efforts (Frame and Hu, 1991a and 1991b; Portner and Shafer, 1996)), many animal cell models have been developed. The common limitation of the available models is that they have focused on characterizing only selected aspects of the overall cell metabolism. Gombert and Nielsen (2000) reviewed stoichiometry-based models versus dynamic models based on empirical kinetics. The key advantage of the stoichiometry-based models is that they account for competing reactions, which is useful for describing the metabolic network and for studying the relative activity of certain pathways under various culture conditions. However, they are unable to incorporate regulation and control of cellular activity, which could be achieved by dynamic models based on the reaction kinetics. The authors concluded that dynamic models are not so widespread in literature and are usually applied to the analysis of relatively small aspects of the metabolism. Sidoli et al. (2004) reviewed the developments in the modeling of mammalian cell cultures in the past decade, with focus on two types of mathematical models. To describe a population of cells consisting of multiple populations with distributed properties within a culture, population balance model (PBM) has been proposed. However, PBMs have not been widely used because of two major problematic features. First, they are complicated to solve and to employ for optimization purposes. Second, accurate determination of the model parameters is seriously limited due to lack of proper measurements. Thus, the single cell model (SCM) has been generally chosen over PBM models for modeling these systems.

Due to exacting nutritional requirements and complex physiology, it is particularly challenging to develop dynamic mathematical models for animal cell culture. It should be noted that often the metabolites to be modeled by the macroscopic equations are preselected (e.g., glucose or glutamine) and the interactions between them are assigned arbitrarily. If all of the interactions of the metabolites and cell physiology are included, the dimension of the model may be too large for the purpose of model-based optimization and control. Thus, to achieve model simplification, macroscopic modeling of biological cell cultures often involves an a priori selection of the elementary reaction scheme. The main idea is to relate the major macroscopic species, including biomass, essential substrates, and products of interest, by a set of macro reactions. Once the reaction scheme is selected, a systematic model reduction procedure is then required to obtain a macroscopic reaction scheme. This data reduction is essential to obtain a manageable set of equations for optimization purposes. Finally, the reaction kinetics needs to be determined, and the complete dynamic model is then obtained based on the mass balance equations of the macroscopic species involved in the reaction scheme.

Dynamic mathematical models require, beyond the information about the stoichiometry of the biological reaction system, knowledge about the reaction kinetics. The identification of a priori unknown reaction kinetics is often a critical task due to the nonlinearity and over-parametrization of the model equations needed to account for all the possible modulation phenomena. Wouwer and Bogaerts (2005) proposed a general formulation of reaction kinetics, as an extension of the Monod kinetics, which allows limitation, activation, and inhibition to be described with a reduced number of parameters. For illustrative purposes, the reaction kinetics used in the current paper is Monod kinetics. Previous dynamic models for hybridomas were

* To whom correspondence should be addressed. Ph: 519-888-4567 ext. 6980. Fax: 519-746 4979. Email: hbudman@engmail.uwaterloo.ca.

[†] Sanofi Pasteur Limited.

[‡] University of Waterloo.

10.1021/bp060089y CCC: $37.00
Published on Web 01/18/2007

B

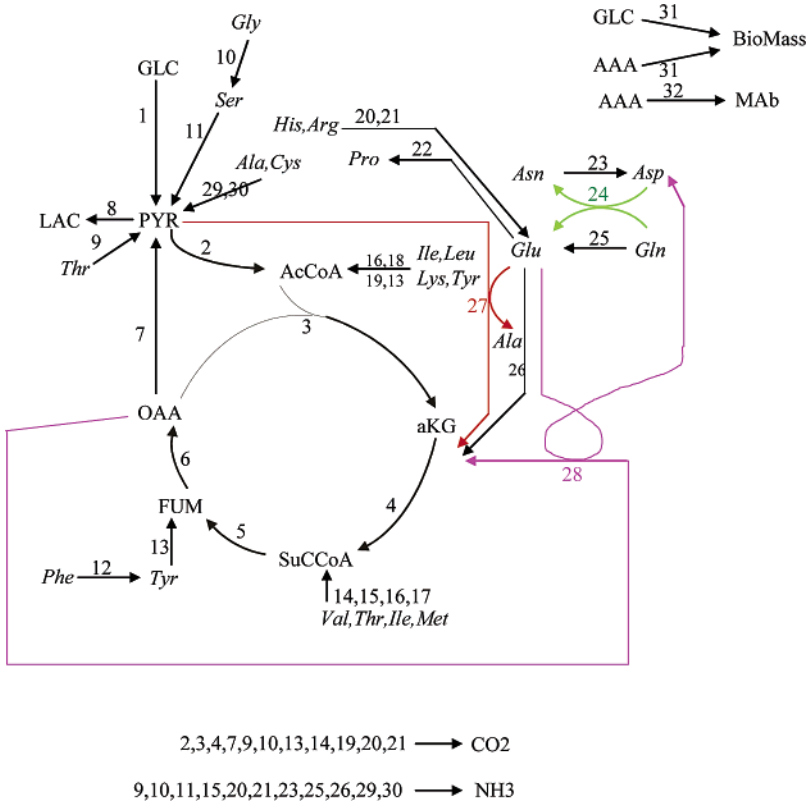

Figure 1. Metabolic network for hybridoma cells.

limited to the exponential growth phase and steady-state continuous culture only (Follstad et al., 1998; Bonarius et al., 1995; Provost and Bastin, 2004; Haag et al., 2005). However, for the purpose of process optimization, the modeling of both the exponential and the post-exponential or declining growth phase will be required. As an expansion to the previous modeling efforts, an approach is proposed to develop a dynamic model for both the exponential phase and the post-exponential phase. Separate models were also obtained recently for different phases of the culture, and a complete model is derived based on the implementation of switching functions by Provost et al. (2006).

To address the above problems, in the current paper, a systematic procedure of developing a dynamic metabolic model is used that is based on the combination of stoichiometric and dynamic mass balances as follows. First, stoichiometric flux balances based on a comprehensive metabolic network description are constructed. This is accomplished by using available process knowledge in combination with experimental or published metabolic information. Intracellular fluxes are calculated using QP from the measured extracellular (transmembrane) fluxes using the stoichiometry of the comprehensive metabolic network. Second, the metabolic network is simplified by systematic elimination of fluxes that are deemed insignificant (smaller than a preset threshold). A set of macro-reactions are identified that directly relate the extracellular metabolites to the products. Finally, kinetic expressions based on Monod kinetics are added to obtain a dynamic model, which includes the regulation of the metabolite uptake or synthesis.

Materials and Methods

Murine hybridoma 130-8F was provided by Sanofi Pasteur Ltd. (Toronto, Canada) and was propagated in D-MEM (Gibco 12100) with 2% FBS (JRH 12107-78P). The medium was supplemented with proline (Sigma P-8449), L-asparagine (Sigma A-4159), and L-aspartic acid (Sigma A-4534). Seed cultures were subcultured on a 3-day regime. Seed and batch cultures were grown in 250 mL and 500 mL spinners in a CO_2 incubator (Sanyo IR Sensor, 37 °C, 8.0% CO_2). Batch cultures were maintained for at least 7 days with frequent sampling.

Viable cell concentration and total cell concentration were determined by the trypan blue exclusion test using a hemocytometer. Glucose, lactate, glutamine, and glutamate concentration was quantified using a YSI analyzer. Ammonia was measured using a Sigma ammonia kit (Sigma 171-B). Total Immunoglobulin titer (MAb concentration) was determined using enzyme linked immunosorbent assay (ELISA) with alkaline phosphatase conjugated goat anti-mouse IgG as the primary reagent. The amino acids in deproteinated medium were derivatized with OPA (*o*-phthaldehyde and 3-mercaptopropionic acid in borate buffer) followed with FMOC (9-fluorenylmethylchloroformate in acetonitrile) and assayed using high performance liquid chromatography (Hypersil AA-ODS column).

Results and Discussion

Metabolic Flux Analysis. Metabolic flux analysis (MFA) refers to calculating unknown intracellular fluxes from measured extracellular fluxes by applying the steady-state mass balance equations. For each metabolite, a mass balance can be derived in which both the transport rates over the cell membrane and the intracellular reaction rates are included. This results in a set of linear equations with a certain number of unknowns. The resulting set of linear equations is usually underdetermined since the number of unknown fluxes is larger than the number of mass balances. To solve such an undetermined network, a quadratic programming (QP) approach has been used in this paper.

Based on published reports (Bonarius et al., 1995; Gambhir et al., 2003; Follstad et al., 1998; Frame and Hu, 1991a and 1991b), the metabolic network shown in Figure 1 is constructed

Table 1. Conversion Rates as Functions of Fluxes

$\mathbf{R}_{exp}$	$\mathbf{R}_{post-exp}$	$\mathbf{R}_{full}$	mass balances of metabolites as functions of fluxes
0	0	0	R1(PYR) = 2j1 − j2+j7 − j8 + j9 + j11 − j27 + j29 + j30
0	0	0	R2(AcCoA) = j2 − j3 + 2j13 + j16 + 3j18 + 2j19
0	0	0	R3(aKG) = j3 − j4 + j21 + j26 + j27 + j28
0	0	0	R4(SuCCoA) = j4 − j5 + j14 + j15 + j16 + j17
0	0	0	R5(FUM) = j5 − j6 + j13
0	0	0	R6(OAA) = −j3 + j6 − j7 − j28
−0.0716	−0.0046	−0.0341	R7(GLC) = −j1 − 0.0208j31
0.0553	−0.0024	0.0226	R8(LAC) = j8
0.1064	0	0.0458	R9(NH_3) = j9 + j10 + j11 + j13 + j14 + j15 + j16 + j17 + j18 + 2j19 + 2j20 + 2j21 + j23 + j25 + j26 + j29 + j30
0.0309	0.0088	0.0191	R10(Ala) = j27 − j30 − 0.0133j31 − 0.011j32
−0.0064	0	−0.0029	R11(Arg) = −j21 − 0.0027j31 − 0.005j32
−0.0070	0.0002	−0.0034	R12(Asp) = j23 − j24 + j28 − 0.0261j31 − 0.0082j32
−0.0045	−0.0037	−0.0032	R13(Asn) = −j23 + j24 − 0.0072j32
−0.0003	−0.0003	−0.0032	R14(Cys) = j29 − 0.0004j31 − 0.005j32
−0.1012	−0.0072	−0.0508	R15(Gln) = −j24 − j25 − 0.0377j31 − 0.0104j32
0.0011	0.0005	0.0004	R16(Glu) = j20 − j22 + j24 + j25 − j26 − j27 − j28 − 0.0006j31 − 0.0107j32
−0.0133	0.0031	−0.0025	R17(Gly) = −2j10 − 0.0165j31 − 0.0145j32
−0.0031	0	−0.0016	R18(His) = −j20 − 0.0033j31 − 0.0035j32
−0.0078	−0.0034	−0.0048	R19(Ile) = −j16 − 0.0084j31 − 0.005j32
−0.0110	−0.0031	−0.0060	R20(Leu) = −j18 − 0.0133j31 − 0.0142j32
−0.0082	−0.0036	−0.0049	R21(Lys) = −j19 − 0.0101j31 − 0.0145j32
−0.0032	0	−0.0016	R22(Met) = −j17 − 0.0033j31 − 0.0028j32
−0.0036	−0.0001	−0.0018	R23(Phe) = −j12 − 0.0055j31 − 0.0072j32
0.0035	0.0021	0.0048	R24(Pro) = j22 − 0.0081j31 − 0.0148j32
−0.0044	−0.0003	−0.0032	R25(Ser) = j10 − j11 − 0.0099j31 − 0.0267j32
−0.0072	−0.0007	−0.0033	R26(Thr) = −j9 − j15 − 0.008j31 − 0.0267j32
−0.0036	−0.0002	−0.0019	R27(Tyr) = j12 − j13 − 0.004j31 − 0.0085j32
−0.0092	−0.0021	−0.0049	R28(Val) = −j14 − 0.0096j31 − 0.0189j32
0.6574	0.1294	0.3161	R29(BioMass) = j31
4.7425×10^{-6}	8.0402×10^{-6}	5.9958×10^{-6}	R30(MAb) = j32 (MW = 1.5×10^5 g/mol)

with the significant metabolic pathways in proliferating animal cells. This network is used to calculate the flux distribution. In the network, the number on the arrows refers to the corresponding intracellular and transmembrane fluxes totaling $n = 32$ fluxes. The corresponding set of the cellular reactions involved in this network is summarized in Table 6. Reactions 31 and 32 for the biomass and murine MAb production are adapted from the work of Gambhir and et al. (2003). The relative concentrations of some medium components in the biomass were slightly adjusted to correspond to the measured external fluxes. This adjustment is to accommodate the requirements of the cell line and needed to be done just once. The coefficients as shown in Table 6 remain fixed during the current work.

The conversion rate R of a metabolite M in a biological system is given by the sum of the products of the stoichiometric coefficients by the corresponding metabolic fluxes for all of the respective reactions where M is involved, as follows:

$$R(M) = \sum_i \alpha_{i,M} j_i \tag{1}$$

where $\alpha_{i,M}$ is the stoichiometric coefficient of metabolite M in reaction i, and j_i is the intracellular flux through reaction i. A negative value of $\alpha_{i,M}$ indicates that metabolite M is consumed in reaction i, whereas a positive value of $\alpha_{i,M}$ indicates that metabolite M is produced. Thus, eq 1 represents mass balance for each metabolite. The entire set of mass balance equations for the network is given in Table 1. This complete set of equations is obtained based on the cellular reactions given in Table 6. For example, for a metabolic network with m metabolites and n unknown fluxes, the mass balance equations in Table 1 can be expressed in the matrix form as follows:

$$\mathbf{R} = \mathbf{A}\mathbf{j} \tag{2}$$

where $\mathbf{A}$ is the stoichiometric matrix obtained from the reactions listed in Table 1, $\mathbf{j}$ is the vector of unknown fluxes, and $\mathbf{R}$ is the vector of the uptake rates and production rates of all the intracellular and the extracellular metabolites, which can be calculated from experimental measurements as explained as follows.

The mass balance equations for the culture can be written in matrix form in the following manner:

$$\frac{d\boldsymbol{\psi}(t)}{dt} = \mathbf{R}X(t) \tag{3}$$

where $\boldsymbol{\psi}$ is the vector of concentrations, based on culture volume, of all of the intracellular metabolites (R_i, $i = 1, ..., 6$) and the extracellular metabolites (R_i, $i = 7, ..., 30$), t is culture time, and X is the viable cell concentration. The conversion rates of the intracellular metabolites R_i, $i = 1, ..., 6$ are set to zero based on the assumption that under the balanced growth condition, the internal metabolites are at a quasi-steady state. To obtain the values of $\mathbf{R}$ for the extracellular metabolites from experimental data, eq 3 is integrated as follows:

$$\frac{d\boldsymbol{\psi}(t)}{dt} = \mathbf{R}X(t) \xrightarrow{\int} \int_0^t d\boldsymbol{\psi}(t) = \mathbf{R}\int_0^t X(t)\, dt$$

$$\Rightarrow \boldsymbol{\psi}_t - \boldsymbol{\psi}_0 = \mathbf{R}(CH_t - CH_0) \tag{4}$$

where CH is the cumulative volumetric cell-hours (Dutton et al., 1998) defined as

$$CH = \int_0^t X\, dt \tag{5}$$

As shown in eq 4, the instantaneous value of $\mathbf{R}$ is the slope relating the metabolite concentration to the cumulative volumetric cell-hours. The use of the cumulative volumetric cell-hours concept allows for assessment of the productivity and the biological capacity for production on the same cumulative basis (Dutton et al., 1998). An average value of the cumulative

volumetric cell-hours was calculated by using the logarithmic mean cell density between data points as follows:

$$CH = \sum_{0}^{t} \left\{ \frac{X_{t+\Delta t} - X_t}{\ln(X_{t+\Delta t}/X_t)} \times (t_{t+\Delta t} - t_t) \right\} \qquad (6)$$

For the cell line under study, the calculated values of **R** by eq 6 are given in Table 1. Different average values of **R** were calculated from eq 6 according to the different phase of the batch as follows, $\mathbf{R}_{exp}$ for the exponential phase, $\mathbf{R}_{post-exp}$ for the post-exponential phase, and $\mathbf{R}_{full}$ for the entire batch.

Finally, the fluxes **j** can be calculated from the reaction rates **R** by using the matrix equation (eq 2). In the present case this equation is slightly underdetermined since there are more unknown intracellular fluxes than available measurements of extracellular fluxes, i.e. $m < n$. In addition, the reactions, as written, are irreversible, and this fact imposes that the fluxes will be either positive or zero, i.e., $\mathbf{j} \geq 0$. An optimization approach employing quadratic programming has been used in this work to solve the problem where the underdetermined system of equations defined by eq 2 together with the corresponding constraints of the fluxes can be formulated as follows:

$$\text{Min}\{(\mathbf{Aj} - \mathbf{R})^{\mathbf{T}}(\mathbf{Aj} - \mathbf{R})\} \quad \text{s.t. } \mathbf{j} \geq 0 \qquad (7)$$

The chosen cost function in eq 7, i.e. the sum of squared errors, is justified by the fact that the solution will try to extract fluxes from noisy measured reaction rates. Also, although the system under consideration is slightly undetermined, which can lead to infinite possible solutions, if the number of active constraints is larger than the indeterminacy of the system, then the solution to the problem posed in eq 7 is unique. The indeterminacy is determined by subtracting the number of equations from the number of unknowns, e.g., for the current case the indeterminacy is 32 unknowns − 30 equations = 2. Thus, if the number of active constraints is larger than 4, the solution to the QP is unique. Using the average values of $\mathbf{R}_{exp}$ for the exponential phase, $\mathbf{R}_{post-exp}$ for the post-exponential phase, and $\mathbf{R}_{full}$ for the full batch given in Table 1, the corresponding intracellular fluxes obtained from the quadratic programming solution of eq 7 are given in Table 2.

It appears from Table 2 that the fluxes during the exponential phase, $\mathbf{j}_{exp}$, are proportionally larger than either the average fluxes for the entire batch, $\mathbf{j}_{full}$, or the mean fluxes during the post-exponential phase, $\mathbf{j}_{post-exp}$. This indicates that during the exponential phase, the cell division requires much more energy than during the post-exponential phase. The fluxes that are below 0.4% of the sum of the fluxes in each phase correspond to the pathways that are insignificant regarding energy generation in the metabolic network, and they are only involved in biomass and MAb formation. Of the original 32 fluxes it is found that fluxes j_i, $i = 9-21, 26, 29, 32$, are non-significant during the exponential phase; fluxes j_i, $i = 8-22, 26, 28-30, 32$ are not significant during the post-exponential phase; and fluxes j_i, $i = 9-21, 26, 29, 30, 32$ are non-significant during the entire culture. However, flux j_{32} is the flux for MAb production, so it is important and cannot be neglected even if it is relatively smaller than the other fluxes. In conclusion, fluxes j_i, $i = 9-21, 26, 29, 30$ are the non-significant fluxes and were eliminated. The sum of the neglected fluxes amounted to approximately 1% of the total. The simplified metabolic network with the remaining significant fluxes is given in Figure 2, where the number on the arrows represents the original flux number.

Table 2. Fluxes j (μmol/(10^6 cells·h))

j*n*	$\mathbf{j}_{exp}$	$\mathbf{j}_{post-exp}$	$\mathbf{j}_{full}$
j1	0.0580	0.0022	0.0276
j2	0.0846	0.0047	0.0385
j3	0.0939	0.0047	0.0441
j4	0.1585	0.0110	0.0723
j5	0.1646	0.0111	0.0750
j6	0.1652	0.0111	0.0751
j7	0.0639	0.0065	0.0273
j8	0.0553	0	0.0225
j9	0	0	0
j10	0.0013	0	0
j11	0	0	0
j12	0	0	0
j13	0.0006	0	0
j14	0.0024	0	0.0012
j15	0.0014	0	0.0001
j16	0.0017	0	0.0015
j17	0.0005	0	0.0000
j18	0.0019	0	0.0011
j19	0.0004	0	0.0003
j20	0	0	0
j21	0.0007	0	0
j22	0.0094	0	0.0081
j23	0.0613	0.0026	0.0155
j24	0.0579	0.0010	0.0137
j25	0.0174	0.0015	0.0238
j26	0.0057	0	0.0002
j27	0.0507	0.0062	0.0242
j28	0.0074	0	0.0038
j29	0.0001	0	0.0024
j30	0.0105	0	0.0002
j31	0.6575	0.1292	0.3162
j32	0.0001	1.4527×10^{-13}	0.0001

Regarding flux 26, an interesting finding of the metabolic flux analysis was that the dominant means of glutamate (Glu) catabolism to α-ketoglutarate (aKG) involved transamination with pyruvate as the cosubstrate rather than deamination. This explained the significant accumulation of alanine (Ala) from pyruvate and the relatively low level of ammonia formation during the growth phase.

To assess the sensitivity of the flux values to noise in the reaction rates, the vector of measured **R** values was augmented with additional 30 values consisting of the measured values ±10% of the measured values to represent noise. Following this, the QP is formulated to solve the 60 resulting equations, corresponding to the selected 60 **R** values, with 32 unknown fluxes. This over-determined system of equations was solved with a QP solution. The conclusion from this calculation is that the dominant fluxes were exactly the same as the ones calculated using the original vector of 30 rates alone presented in the manuscript. To describe the sensitivity of the results to noise, flux fractions (= flux/sum of fluxes) were calculated and plotted in Figure 3 for the QP using 30 **R** values and 60 **R** values respectively. The figure shows that the differences between these two QP solutions are minimal in terms of the flux fractions

Macroscopic Reaction Scheme. Significant progress has been achieved toward systematic selection of the reaction scheme. Hulhoven et al. (2005) addressed this modeling problem and aimed at the development of a method for systematically evaluating all potential reaction schemes that contain identifiable parameters. Nernard and Bastin (2005) have also summarized the approach of identifying a reaction network, and the authors have applied the approach to a few case studies (Nernard and Bastin, 2005; Provost and Bastin, 2004). They claimed that the results of the procedure may not be unique and a careful examination for complex metabolic networks is necessary.

The reaction scheme given in Figure 2 represents a network that is the combination of the elementary flux modes, also called

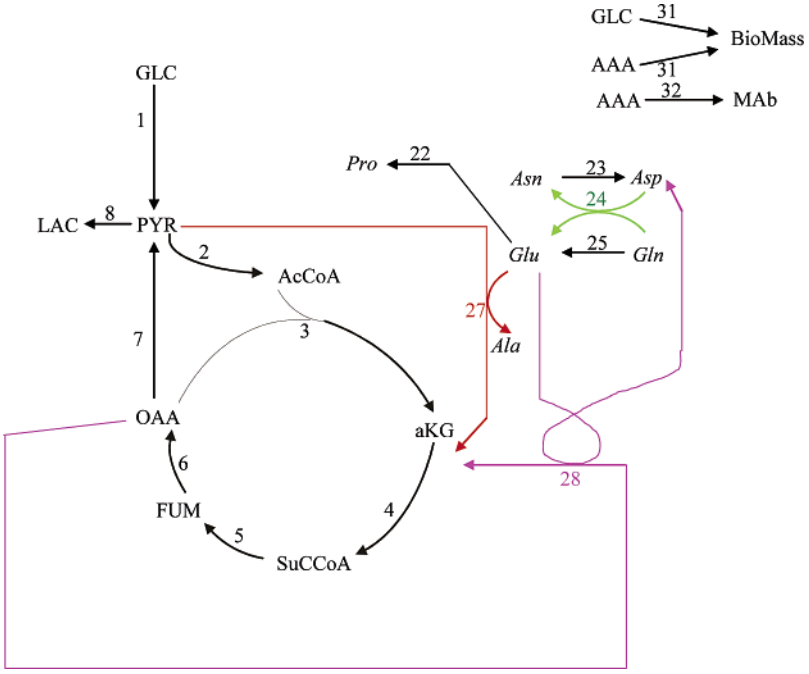

Figure 2. Reduced metabolic network for 130-8F hybridoma cells.

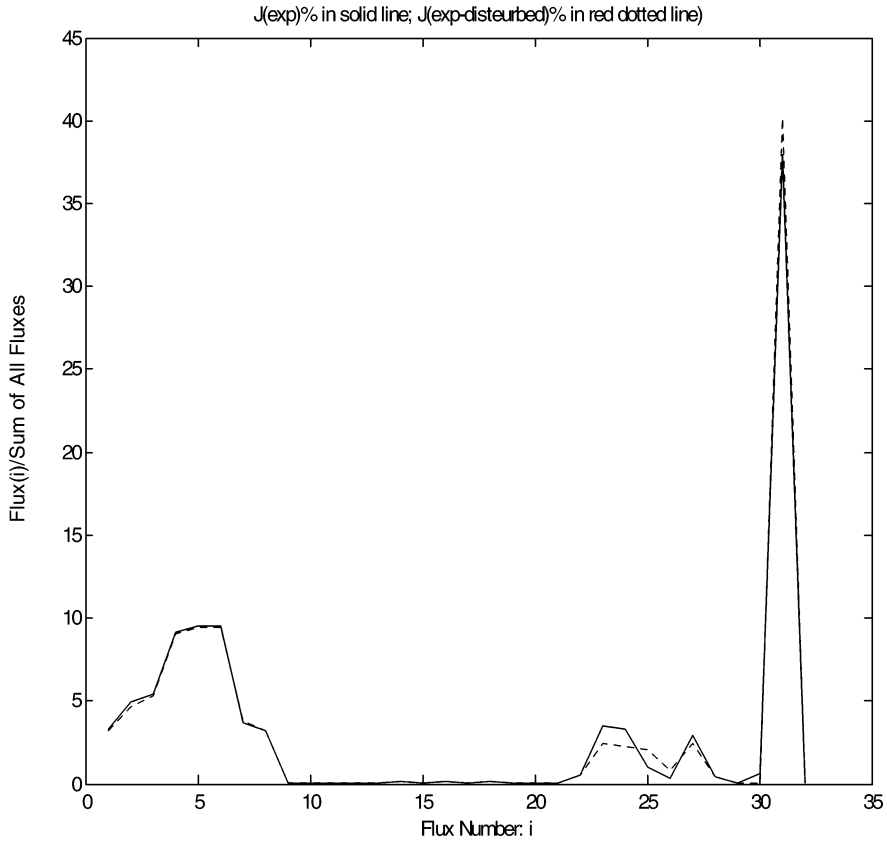

Figure 3. Flux values calculated with the original 30 experimental values (solid line) and with a combination of experimental and perturbed reaction rates values (dash line).

the spanning pathways (Provost and Bastin, 2004). Elementary flux modes are the simplest metabolic paths that are able to connect the substrates to the products, i.e., measurable inputs to outputs. In general, the procedure to determine the elementary flux modes is to minimize the number of unmeasured metabolic variables by appropriate combination of the stoichiometric equations. An efficient automatic C-program Metatool has been used to accomplish this by Provost and Bastin (2004). When the number of fluxes is relatively small, however, judicious combination of equations representing metabolic sequences can be applied to accomplish the same. For the simplified metabolic network shown in Figure 2, the 17 significant metabolic fluxes were combined to give the nine elementary flux modes manually, as summarized in Table 3.

For the purpose of dynamic modeling of extracellular metabolites, the intracellular metabolites are eliminated from

Table 3. Elementary Flux Modes

E1	J1	GLC → 2PYR
	J8	PYR → LAC
	total	GLC → 2LAC
E2	J1	GLC → 2PYR
	J27	PYR + GLU → Ala + aKG
	J4	aKG → SuCCoA + CO_2
	J5	SuCCoA → FUM
	J6	FUM → OAA
	J7	OAA → PYR
	J8	PYR → LAC
	total	GLC + 2GLU→ 2Ala + 2CO_2 + 2LAC
E3	J1	GLC → 2PYR
	J2	PYR → AcCoA + CO_2
	J3	AcCoA + OAA → aKG + CO_2
	J4	aKG → SuCCoA + CO_2
	J5	SuCCoA → FUM
	J6	FUM → OAA
	J28	GLU + OAA → ASP + aKG
	J4	aKG → SuCCoA + CO_2
	J5	SuCCoA → FUM
	J6	FUM → OAA
	J7	OAA → PYR
	J8	PYR → LAC
	total	GLC + 2GLU → 2Asp + 2LAC + 6CO_2
E4	J22	GLU → PRO
	total	GLU → PRO
E5	J23	ASN → ASP + NH_3
	total	ASN → ASP + NH_3
E6	J24	GLN + ASP → ASN + GLU
	total	GLN + ASP → ASN + GLU
E7	J31	0.0208GLC + 0.0377GLN + 0.0133ALA + 0.007ARG + 0.0ASN + 0.026lASP + 0.0004CYS + 0.0006GLU + 0.0165GLY + 0.0033HIS +0.0084ILE + 0.0133LEU + 0.010lLYS + 0.0033MET + 0.0055PHE + 0.0081PRO + 0.0099SER + 0.008THR + 0.004TYR + 0.0096VAL → BioMass
	total	same as above
E8	J32	0.0104GLN + 0.01lALA + 0.005ARG + 0.0072ASN + 0.0082ASP + 0.005CYS + 0.0107GLU + 0.0145GLY + 0.0035HIS + 0.005ILE + 0.0142LEU + 0.0145LYS + 0.0028MET + 0.0072PHE + 0.0148PRO +0.0267SER + 0.0160THR + 0.0085TYR + 0.0189VAL → MAb
	total	same as above
E9	J25	GLN → GLU + NH_3
	Total	GLN → GLU + NH_3

each elementary mode to generate a macro-reaction. For example, for the first elementary mode (e1), the final macro reaction is obtained by adding up reaction j1 and j8 (multiplied by 2 for the elimination of PYR). A total of nine fundamental macro-reactions connecting the extracellular substrates and products are summarized in Table 4.

Reaction Kinetics and Dynamic Model. The dynamic model to describe the mass balances of the extracellular species is given by the following equation:

$$\frac{d\xi(t)}{dt} = \mathbf{K}\mathbf{r}(t) + \mathbf{u}(t) \tag{8}$$

$\boldsymbol{\xi}(t) = (\xi_1 \cdots \xi_p)^T$ is the vector of the extracellular species concentrations; $\mathbf{r}(t) = (r_1 \cdots r_q)^T$ is the vector of the macro-reaction rates; **K** is the stoichiometric matrix of the macro-reaction network; and $\mathbf{u}(t)$ is the input vector representing the net exchange of the species with the surroundings. The term $u_i(t)$ is zero for all species except for CO_2, i.e., the CO_2 gaseous flow rate. However, it should be noted that in this paper CO_2 measurements are not available and CO_2 is not predicted by the model.

The significant metabolites for the hybridoma cell line under study were identified to be the 11 extracellular metabolites involved in the reduced network given in Figure 2, and they

Table 4. Fundamental Macro-Reactions

E1	GLC → 2LAC
E2	GLC + 2GLU → 2Ala + 2CO_2 + 2LAC
E3	GLC + 2GLU → 2Asp + 2LAC + 6CO_2
E4	GLU → PRO
E5	ASN → ASP + NH_3
E6	GLN + ASP → ASN + GLU
E7	0.0508GLC + 0.0577GLN + 0.0133ALA + 0.007ARG + 0.006ASN + 0.020lASP + 0.0004CYS + 0.0016GLU + 0.0165GLY + 0.0033HIS + 0.0084ILE + 0.0133LEU + 0.010lLYS + 0.0033MET + 0.0055PHE + 0.0081PRO + 0.0099SER + 0.008THR + 0.004TYR + 0.0096VAL → BioMass
E8	0.0104GLN + 0.01lALA + 0.005ARG + 0.0072ASN + 0.0082ASP + 0.005CYS + 0.0107GLU + 0.0145GLY + 0.0035HIS + 0.005ILE + 0.0142LEU + 0.0145LYS + 0.0028MET + 0.0072PHE + 0.0148PRO + 0.0267SER + 0.0160THR + 0.0085TYR + 0.0189VAL → MAb
E9	GLN → GLU + NH_3

were put in the following vector $\boldsymbol{\xi}(t)$:

$$\xi = (GLC(G), GLN(Q), LAC(L), GLU(U), ASN(S), ASP(F), ALA, PRO, BioMass, MAb)^T \tag{9}$$

where the single letter in the bracket after each metabolite is a symbol used to represent that metabolite for simplicity, e.g., U for glutamate.

Table 5. Reaction Rates of Macro-Reactions

no.	reaction	rate expression	parameters
E1	GLC(G) → 2LAC	$r_i = a_i \frac{GX}{k_{Gi} + G}, i = 1$	a_1, k_{G1}
E2	GLC(G) + 2GLU(U) → 2Ala + 2CO_2 + 2LAC	$r_i = a_i \frac{GUX}{(k_{Gi} + G)(k_{Ui} + U)}, i = 2, 3$	a_2, k_{G2}, k_{U2}
E3	GLC(G) + 2GLU(U) → 2Asp + 2LAC + 6CO_2		a_3, k_{G3}, k_{U3}
E4	GLU(U) → PRO	$r_i = a_i \frac{UX}{(k_{Ui} + U)}, i = 4$	a_4, k_{U4}
E5	ASN(S) → ASP + NH_3	$r_i = a_i \frac{SX}{k_{Si} + S}, i = 5$	a_5, k_{S5}
E6	GLN(Q) + ASP(F) → ASN + GLU	$r_i = a_i \frac{QFX}{(k_{Qi} + Q)(k_{Fi} + F)}, i = 6$	a_6, k_{Q6}, k_{F6}
E7	GLC(G) + AAA → BioMass	$r_i = a_i \frac{Q}{k_{Qi} + Q} X, i = 7$	a_7
E8	AAA → MAb	$r_i = a_i \frac{Q}{k_{Qi} + Q} X, i = 8$	a_8
E9	GLN(Q) → GLU + NH_3	$r_i = a_i \frac{QX}{k_{Qi} + Q}, i = 9$	a_9, k_{Q9}

The stoichiometric matrix **K** is computed directly from Table 4 in combination with the general equation 8 as follows:

$$\mathbf{K} =$$

	r1	r2	r3	r4	r5	r6	r7	r8	r9
GLC	−1	−1	−1	0	0	0	−0.0508	0	0
GLN	0	0	0	0	0	−1	−0.0577	−0.0104	−1
LAC	2	2	2	0	0	0	0	0	0
NH_3	0	0	0	0	1	0	0	0	1
GLU	0	−2	−2	−1	0	1	−0.0016	−0.0107	1
ASN	0	0	0	0	−1	1	−0.006	−0.0072	0
ASP	0	0	2	0	1	−1	−0.0201	−0.0082	0
ALA	0	2	0	0	0	0	−0.0133	−0.011	0
PRO	0	0	0	1	0	0	−0.0081	−0.0148	0
CO_2	0	2	6	0	0	0	0	0	0
BioMass	0	0	0	0	0	0	1	0	0
MAb	0	0	0	0	0	0	0	1	0

$p \times q$ (10)

It is assumed that the reaction rates $r_i(t)$ of the macro-reactions satisfy simple Monod-type kinetics. The rate expressions with the corresponding kinetic parameters are summarized in Table 5. The explicit mass balances for the elements of ξ are

$$\frac{dGLC(t)}{dt} = -a_1 \frac{GX}{k_{G1} + G} - a_2 \frac{GUX}{(k_{G2} + G)(k_{U2} + U)} - a_3 \frac{GUX}{(k_{G3} + G)(k_{U3} + U)} - 0.0508 a_7 \frac{Q}{k_{Q7} + Q} X$$

$$\frac{dGLN(t)}{dt} = -a_6 \frac{QFX}{(k_{Q6} + Q)(k_{F6} + F)} - 0.0577 a_7 \frac{Q}{k_{Q7} + Q} X - 0.0104 a_8 \frac{Q}{k_{Q8} + Q} X - a_9 \frac{QX}{k_{Q9} + Q}$$

$$\frac{dLAC(t)}{dt} = 2a_1 \frac{GX}{k_{G1} + G} + 2a_2 \frac{GUX}{(k_{G2} + G)(k_{U2} + U)} + 2a_3 \frac{GUX}{(k_{G3} + G)(k_{U3} + U)}$$

$$\frac{dNH_3(t)}{dt} = a_5 \frac{SX}{k_{S5} + S} + a_9 \frac{QX}{k_{Q9} + Q}$$

$$\frac{dGLU(t)}{dt} = -2a_2 \frac{GUX}{(k_{G2} + G)(k_{U2} + U)} - 2a_3 \frac{GUX}{(k_{G3} + G)(k_{U3} + U)} - a_4 \frac{UX}{k_{U4} + U} + a_6 \frac{QFX}{(k_{Q6} + Q)(k_{F6} + F)} - 0.0016 a_7 \frac{Q}{k_{Q7} + Q} X - 0.0107 a_8 \frac{Q}{k_{Q8} + Q} X + a_9 \frac{QX}{k_{Q9} + Q}$$

$$\frac{dASN(t)}{dt} = -a_5 \frac{SX}{k_{S5} + S} + a_6 \frac{QFX}{(k_{Q6} + Q)(k_{F6} + F)} - 0.006 a_7 \frac{Q}{k_{Q7} + Q} X - 0.0072 a_8 \frac{Q}{k_{Q8} + Q} X$$

$$\frac{dASP(t)}{dt} = 2a_3 \frac{GUX}{(k_{G3} + G)(k_{U36} + U)} + a_5 \frac{SX}{k_{S5} + S} - a_6 \frac{QFX}{(k_{Q6} + Q)(k_{F6} + F)} - 0.0201 a_7 \frac{Q}{k_{Q7} + Q} X - 0.0082 a_8 \frac{Q}{k_{Q8} + Q} X$$

$$\frac{dALA(t)}{dt} = 2a_2 \frac{GUX}{(k_{G2} + G)(k_{U2} + U)} - 0.0133 a_7 \frac{Q}{k_{Q7} + Q} X - 0.011 a_8 \frac{Q}{k_{Q8} + Q} X$$

$$\frac{dPRO(t)}{dt} = a_4 \frac{UX}{k_{U4} + U} - 0.0081 a_7 \frac{Q}{k_{Q7} + Q} X - 0.0148 a_8 \frac{Q}{k_{Q8} + Q} X$$

$$\frac{dBioMass(t)}{dt} = a_7 \frac{Q}{k_{Q7} + Q} X$$

$$\frac{dMAb(t)}{dt} = a_8 \frac{Q}{k_{Q8} + Q} X \quad (11)$$

Parameters a_i are the maximum specific reaction rates and are very important parameters of the model, and k_{Gi}, k_{Qi}, k_{Ui}, k_{Si}, k_{Fi} are the half-saturation constants. AAA in reactions 7

Table 6. Stoichiometric Equations

j*n*	reaction
j1	GLC → 2PYR + 2NADH + 2ATP
j2	PYR → AcCoA + CO_2 + NADH
j3	AcCoA + OAA → aKG + NADH + CO_2
j4	aKG → SuCCoA + NADH + CO_2
j5	SuCCoA → FUM + NADH
j6	FUM → OAA + NADH
j7	OAA → PYR + NADPH + CO_2
j8	PYR + NADH → LAC
j9	THR → PYR + CO_2 + NH_3 + 2NADH
j10	2GLY → SER + CO_2 + NH_3 + NADH
j11	SER → PYR + NH_3
j12	PHE → TYR + NADH
j13	TYR → FUM + 2AcCoA + NH_3 + CO_2 + NADPH
j14	VAL → SuCCoA + CO_2 + NH_3 + NADPH
j15	THR → SuCCoA + NH_3
j16	ILE → SuCCoA + AcCoA + NADPH + NH_3
j17	MET + O_2 → SuCCoA + SO_2 + NADPH + NH_3
j18	LEU → NH_3 + 3AcCoA + NADPH
j19	LYS → 2AcCoA + 2CO_2 + 2NADPH + 2NH_3
j20	HIS → GLU + 2NH_3 + CO_2
j21	ARG → aKG + 2NH_3 + urea + 3NADH
j22	GLU + ATP + 2NADPH → PRO
j23	ASN → ASP + ATP + NH_3
j24	GLN + ASP + 2ATP → ASN + GLU
j25	GLN → GLU + ATP + NH_3
j26	GLU → AKG + NADPH + NH_3
j27	PYR + GLU → ALA + AKG
j28	GLU + OAA → ASP + AKG
j29	CYS + O_2 → PYR + SO_2 + NADH + NH_3
j30	ALA → PYR + NADH + NH_3
j31	0.0508GLC + 0.0577GLN + 0.0133ALA + 0.007ARG + 0.006ASN + 0.020lASP + 0.0004CYS + 0.0016GLU + 0.0165GLY + 0.0033HIS + 0.0084ILE + 0.0133LEU + 0.010lLYS + 0.0033MET + 0.0055PHE + 0.0081PRO + 0.0099SER + 0.008THR + 0.004TYR + 0.0096VAL → BioMass
j32	0.0104GLN + 0.01lALA + 0.005ARG + 0.0072ASN + 0.0082ASP + 0.005CYS + 0.0107GLU + 0.0145GLY + 0.0035HIS + 0.005ILE + 0.0142LEU + 0.0145LYS + 0.0028MET + 0.0072PHE + 0.0148PRO + 0.0267SER + 0.0160THR + 0.0085TYR + 0.0189VAL → MAb

and 8 represents all the amino acids; the corresponding reactions are written in their complete form in Table 4.

The model parameters a_i and k_{Gi}, k_{Qi}, k_{Ui}, k_{Si}, k_{Fi} given in eq 8 need to be determined before the model can be applied for prediction. The number of equations given in expression 11 is 13, whereas there are 19 parameters to be determined. This underdetermined problem has no unique solution unless more constraints are defined, and it may not be necessary to identify all 19 parameters from experimental data. The maximum specific reaction rates a_i depend on the experiment conditions and must be identified from experimental data of the metabolites and biomass, whereas the half-saturation constants can be determined using the balanced-growth assumption.

The main purpose of the model is to predict the key metabolite consumption as well as synthesis of viable cells. Under balanced growth conditions, the macro-reactions can be assumed to proceed at their maximum rates. The half-saturation constants k_{Gi}, k_{Qi}, k_{Ui}, k_{Si}, k_{Fi} are therefore selected to be sufficiently small compared to the metabolite concentration, as shown in eq 12. During the growth phase when the metabolite concentrations far exceed the value of the half-saturation constant, the reaction rate r becomes essentially equal to the maximum specific reaction rate, a. For example, the first reaction in Table 5, $r_i = a_i GX/(k_{Gi} + G)$, $i = 1$becomes $r_i = a_i X$, $i = 1$ when $r_i = \gg k_{Gi}$, $i = 1$. Only during the death phase when the metabolite concentrations are very small and comparable to the half-saturation constant, the reaction rate r needs to be determined explicitly by considering the half-saturation constants. The half-saturation constants are kept in a range that provides maximum rates during the exponential phase but avoids numerical stiffness to prevent computational problems during modeling. It should be noted that because the small half-saturation constants for the post-exponential phase are assumed to be the same as for the exponential phase, the reactions are assumed to be of zero order for the post-exponential phase as well. The half-saturation constants k_{Gi}, k_{Qi}, k_{Ui}, k_{Si}, k_{Fi} are chosen to be

$$k_{Gi} = k_{Qi} = 0.01 \text{ (mmol/L)}$$

$$k_{Ui} = k_{Si} = k_{Fi} = 0.0001 \text{ (mmol/L)} \tag{12}$$

As a result, the following is true:

$$G \gg k_{Gi}, Q \gg k_{Qi}, U \gg k_{Ui}, S \gg k_{Si}, F \gg k_{Fi} \tag{13}$$

Using the assumed small values in eq 12, then

$$r_i(t) \cong a_i X(t),\ \mathbf{r}(t) \cong \mathbf{a}X(t) \tag{14}$$

Then, the dynamic model from eq 8 can be rewritten as

$$\frac{\mathrm{d}\xi(t)}{\mathrm{d}t} = \mathbf{K}\mathbf{r}(t) \xrightarrow{\mathbf{r}(t) = \mathbf{a}X(t)} \frac{\mathrm{d}\xi(t)}{\mathrm{d}t} = \mathbf{K}\mathbf{a}X(t) \tag{15}$$

The mass balance equations for the metabolites in the vector ξ can be written as follows:

$$\frac{\mathrm{d}\xi(t)}{\mathrm{d}t} = \mathbf{R}_\xi X(t) \tag{16}$$

where $\mathbf{R}_\xi$ is the vector of the uptake and production rates of the extracellular metabolites ξ. Comparing eqs 15 and 16, the parameters **a** can be identified as non-negative solution of the linear relationship between the measured specific uptake and excretion rates $\mathbf{R}_\xi$ and the maximum macro-reactions rates a_i, given by

$$\mathbf{R}_\xi = \mathbf{K}\mathbf{a} \tag{17}$$

As illustrated in the section of the metabolic flux analysis, the uptake and production rates $\mathbf{R}_\xi$ of the extracellular metabolites ξ can be calculated from the linear regression of the metabolite concentrations and cumulative volumetric cell-hours using eq 4. $\mathbf{R}_\xi$ consists only of a part of the vector **R**, with only the elements corresponding to the metabolites in the vector ξ defined by eq 9. If some measurements of metabolites in the vector ξ are not available from the experiments, then the corresponding rows of the matrix **K**, defined by eq 10, can be taken out of this matrix. Thus, the missing data will not affect the identification of the maximum reaction rates a_i. For example, if NH_3 data are not available, the fourth row is eliminated from the matrix **K**.

The results in Table 1 show that the cell-specific uptake/excretion rates are significantly different during the exponential ($\mathbf{R}_{\text{exp}}$) and the post-exponential phase ($\mathbf{R}_{\text{post-exp}}$). Consequently, the vectors $\mathbf{R}_{\xi,\text{exp}}$ and $\mathbf{R}_{\xi,\text{post-exp}}$ will be also different. Consequently, different model parameters $\mathbf{a}_{\text{exp}}$ and $\mathbf{a}_{\text{post}}$ are used for the exponential and for the post-exponential phase respectively. These parameters are identified by applying the QP approach based on the following relationships that result from eq 17:

$$\mathbf{R}_{\xi,\text{exp}} = \mathbf{K}\mathbf{a}_{\text{exp}} \tag{18}$$

$$\mathbf{R}_{\xi,\text{post-exp}} = \mathbf{K}\mathbf{a}_{\text{post-exp}} \tag{19}$$

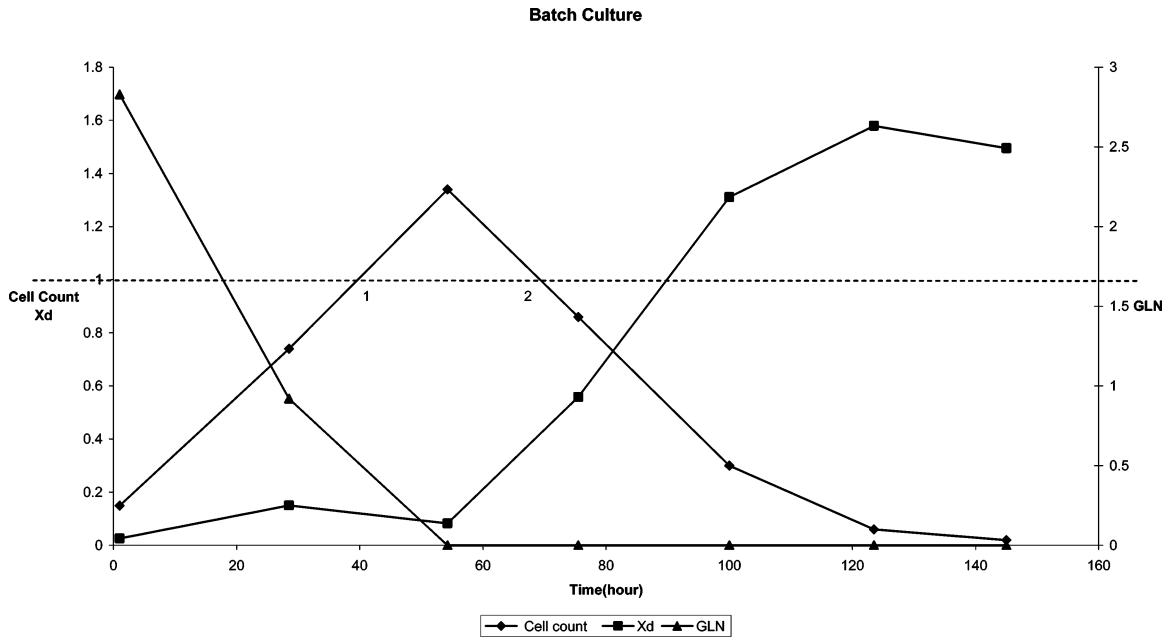

Figure 4. Viable cell and glutamine concentration in batch culture.

Thus, combining eqs 16 and 17, the metabolite mass balance dynamic model can be written as

$$\frac{d\xi(t)}{dt} = \mathbf{K}\mathbf{a}_{exp}X(t) = \mathbf{K}\mathbf{r}_{exp} \text{ for exponential phase} \quad (20)$$

$$\frac{d\xi(t)}{dt} = \mathbf{K}\mathbf{a}_{post-exp}X(t) = \mathbf{K}\mathbf{r}_{post-exp} \text{ for post-exponential phase} \quad (21)$$

During the exponential phase, as the number of viable cells increases, a certain amount of nutrients are required for growth, as well as maintenance and metabolite production (Portner and Schafer, 1996). Hence, during the exponential phase, the uptake rates of substrates and the production rates of the metabolites should depend on both the viable cell concentration $X(t)$ and the specific growth rate of the viable cells, $dX(t)/dt = \mu X(t)$. On the other hand, during the post-exponential phase cell growth slows down significantly or ceases and much less nutrients are required for growth and the majority of nutrient requirement is for the maintenance and production. Consequently, during the post-exponential phase, the specific uptake/production rates should depend only on the viable cell concentration, $X(t)$.

Following these arguments it was assumed that

$$\mathbf{a}_{exp} = \mathbf{a}_m + \mathbf{a}_g\mu \quad (22)$$

$$\mathbf{a}_{post-exp} = \mathbf{a}_m \quad (23)$$

where $\mathbf{a}_m$ and $\mathbf{a}_g$ are obtained from eqs 18 and 19 in combination with definitions 22 and 23. Thus $\mathbf{a}_m$ is obtained from the QP solution of the following problem:

$$\mathbf{R}_{\xi,post-exp} = \mathbf{K}\mathbf{a}_m \quad (24)$$

and using $\mathbf{a}_m$ obtained from eqs 24 and 22, the solution for $\mathbf{a}_g$ is derived from

$$\frac{\mathbf{R}_{\xi,exp} - \mathbf{K}\mathbf{a}_m}{\mu} = \mathbf{K}\mathbf{a}_g \quad (25)$$

Then, the dynamic model can be rewritten as

$$\frac{d\xi(t)}{dt} = \mathbf{K}\mathbf{a}_{exp}X(t) = \mathbf{K}(\mathbf{a}_m + \mathbf{a}_g\mu)X(t) \text{ for exponential phase} \quad (26)$$

$$\frac{d\xi(t)}{dt} = \mathbf{K}\mathbf{a}_{post-exp}X(t) = \mathbf{K}\mathbf{a}_mX(t) \text{ for post-exponential phase}$$

It should be noted that the same values of the coefficients $\mathbf{a}_m$, used to describe the maintenance, are used for the exponential and post-exponential phase.

To complete the mathematical model, it is necessary to predict the viable cell concentrations of the culture, because the metabolite mass balances depend on the amount of the viable cells based on the model structure given in eq 16. Typical growth and post-exponential decline of viable cells in batch culture is shown in Figure 4. After reaching a maximum value, the overall viable cell concentration begins to decline as the culture enters the post-exponential (apoptotic) phase. It is desirable to have a model that is able to predict the onset of cell population decline. With this objective in mind the following model was proposed:

for the growth phase

$$\frac{dX}{dt} = \mu X - (k_oX_d)X$$

$$\frac{dX_d}{dt} = k_oXX_d \quad (27)$$

and for the post-exponential phase

$$\frac{dX}{dt} = -(k_oX_d)X$$

$$\frac{dX_d}{dt} = k_oXX_d \quad (28)$$

where X_d is the dead cell concentration, and k_o is a model parameter identified from the experimental data using the nonviable cell equation given in eq 27.

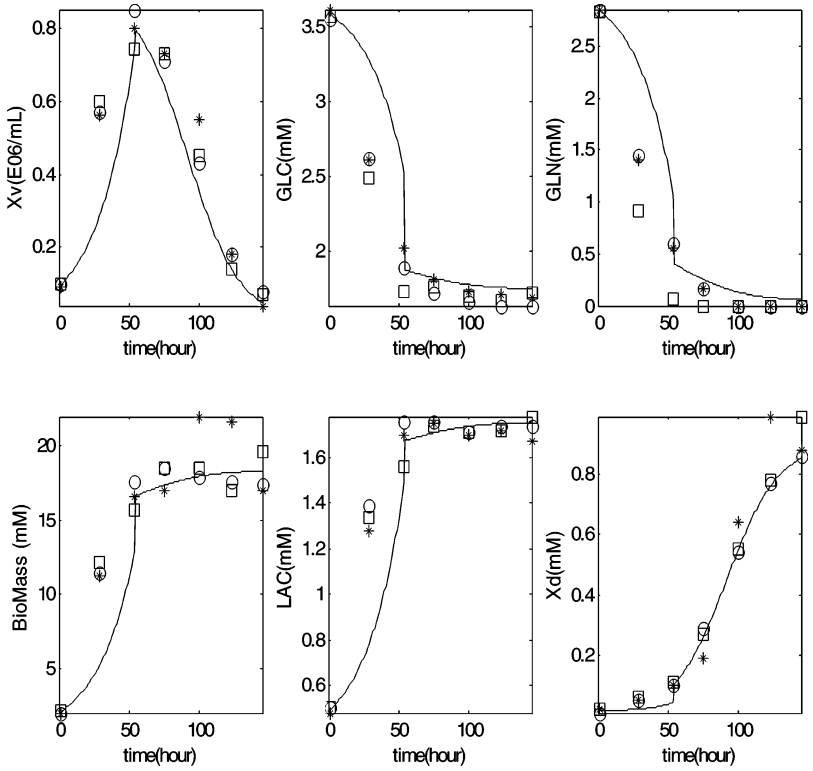

Figure 5. Comparison of model calibration prediction using average rates (−) versus the data used for model calibration (○, □, ∗).

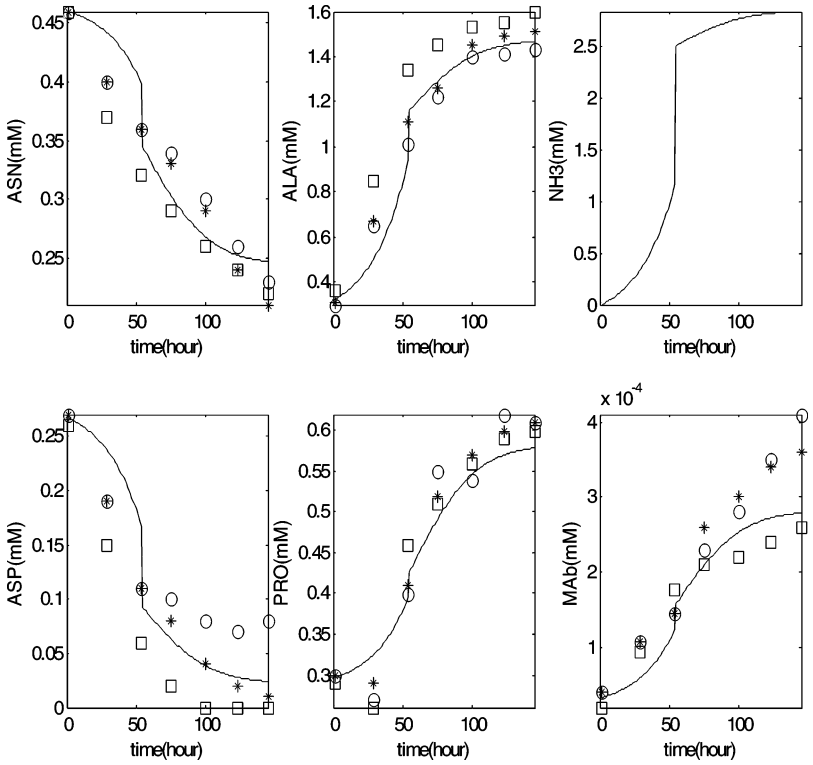

Figure 6. Comparison of model calibration prediction using average rates (−) versus the data used for model calibration (○, □, ∗).

The model of viable cell concentration given in eqs 27 and (28) includes a cell growth inhibition term $k_o X_d$. The rationale behind this term is that cell death is related to some toxin or inhibitor concentration that is proportional to the concentration of nonviable cells. Since this term enters the equations with a negative sign and since the non-viable cell concentration is continuously increasing, it correctly models the experimental observation that cell proliferation cannot be re-established by feeding of fresh nutrients once the cells in a culture are committed to apoptosis. A more detailed model of the onset and evolution of cell apoptosis and necrosis is beyond the scope of the current study. The current proposed model was deemed sufficiently accurate for the purpose of fitting the experimental data as shown in the following section.

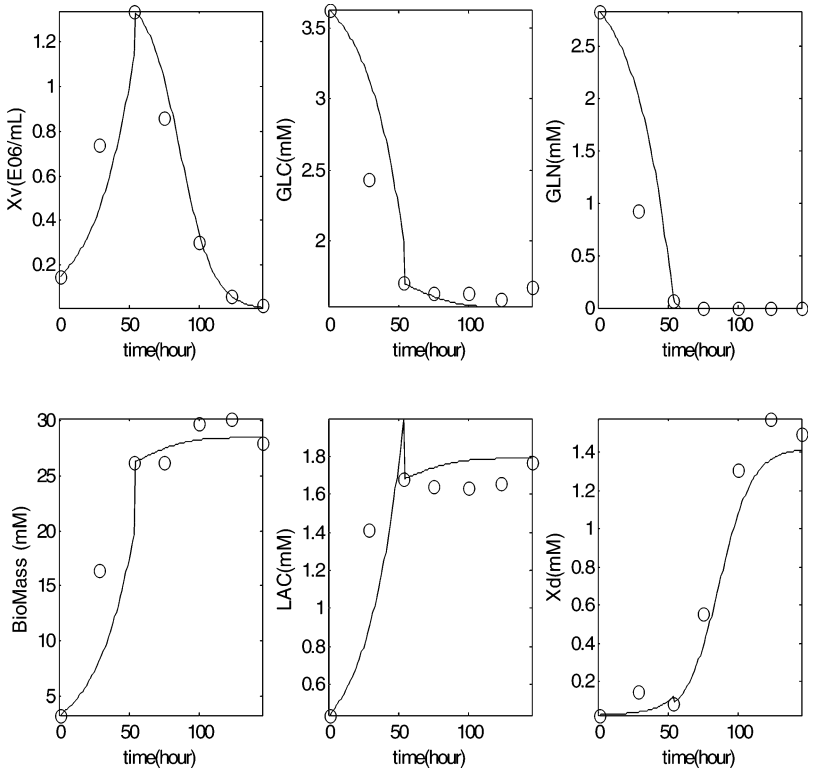

Figure 7. Comparison of model predictions (−) versus batch 1 of the testing data (○) (growth rate $\mu_1 = 0.042$ h^{-1}).

In summary, based on eq 26 the dynamic model with a total of 13 differential equations is given by the following equations:

$$\frac{d\xi(t)}{dt} = \mathbf{Ka}_{exp}X(t) \text{ or } \frac{d\xi(t)}{dt} = \mathbf{Ka}_{post-exp}X(t) \qquad (29)$$

$$\frac{dX}{dt} = \mu X - k_o XX_d(\text{exp}) \text{ or } \frac{dX}{dt} = -k_o XX_d(\text{post-exp})$$

$$\frac{dX_d}{dt} = k_o XX_d$$

Model Calibration and Testing. Six independent batch experiments were performed, and the data collected in these experiments were used for calibration and testing of the mathematical model. In four of these experiments the concentrations of viable cells, total number of cells and amino acids, glucose, lactate, and MAb were determined. In the remaining two experiments only viable cells, glucose, non-viable cells, and lactate concentrations data were collected.

The data were split in two sets of three batches each. The first set of three batches was used for calibration of the model, whereas the second set was used for testing of the accuracy of the mathematical model. One set of metabolite uptake and production rate values are calculated and given by the vector $\mathbf{R}_\xi$ as described in eq 30. The calculation of these values was based on the QP solution of eqs 18 and 19. It should be noted that for the three batches used for calibration the measured growth rates represent a certain amount of variability, i.e., 0.0405, 0.0379, and 0.0413 h^{-1}, respectively. Therefore, to perform the calculations, averaged values of the growth rate and the consumption rates $\mathbf{R}_\xi$ were calculated in order to perform the regression using the QP algorithm, and the values were as follows:

$$\xi = (GLC(G), GLN(Q), LAC(L), GLU(U), ASN(S), ASP(F), ALA, PRO, BioMass, MAb)^T$$

$$\mathbf{R}_{\xi,exp} = [-0.0739\ -0.0987\ 0.0530\ 0.0107\ -0.0044\ -0.0068\ 0.0301\ 0.0034\ 0.6424\ 0.0046]^T$$

$$\mathbf{R}_{\xi,post} = [-0.0054\ -0.0172\ 0.0016\ -0.0002\ -0.0026\ -0.0009\ 0.0112\ 0.0056\ 0.0573\ 0.0077]^T \qquad (30)$$

Using these average values of rates, the model parameters calculated from the QP algorithm were as follows:

$$\mu = 0.0399,\ k_o = 0.06 \qquad (31)$$

$$\mathbf{a}_{exp} = [0.0080\ 0.0191\ 0.0023\ 0.0081\ -0.0100\ -0.0110\ 0.6429\ 0.0046\ 0.0731]$$

$$\mathbf{a}_{post} = [-0.0033\ 0.0058\ -0.0014\ 0.0057\ 0.0056\ 0.0029\ 0.0573\ 0.0077\ 0.0113]$$

$$\mathbf{a}_m = \mathbf{a}_{post}$$

$$\mathbf{a}_g = [0.2840\ 0.3325\ 0.0923\ 0.0596\ -0.7253\ -0.6839\ 14.6764\ -0.0780\ 1.8851]$$

The data collected for the three batches used for calibration (denoted by symbols), together with the model prediction (denoted by solid line), obtained with the averaged reaction rates values, are shown in Figures 5 and 6. Employing the identified parameters, the accuracy of the model was tested by comparing the model predictions with data from the three batches that were not previously used for model calibration.

Using only the knowledge of the measured growth rates ,the model based on the parameters given in eq 31 is used to predict nutrient and metabolic product concentrations. Concentrations of different variables as a function of time for two of the batches used for testing of the models are plotted in Figures 7 and 8 for the first and Figure 9 for a second batch, respectively. For the testing data certain variability in growth rates was obtained

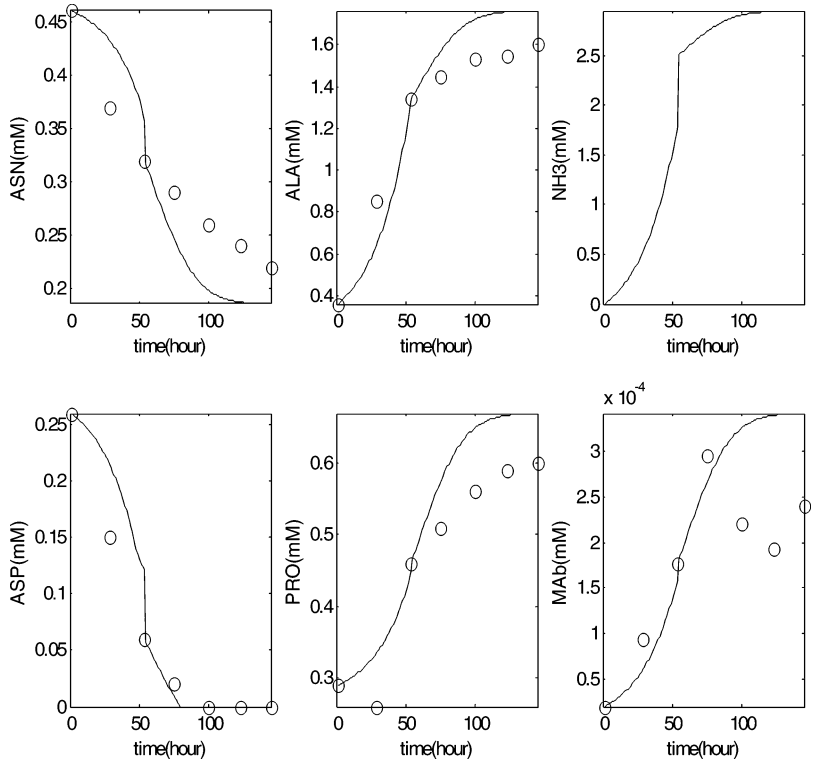

Figure 8. Comparison of model predictions (−) versus batch 1 of the testing data (○) (growth rate $\mu_1 = 0.042\ h^{-1}$)

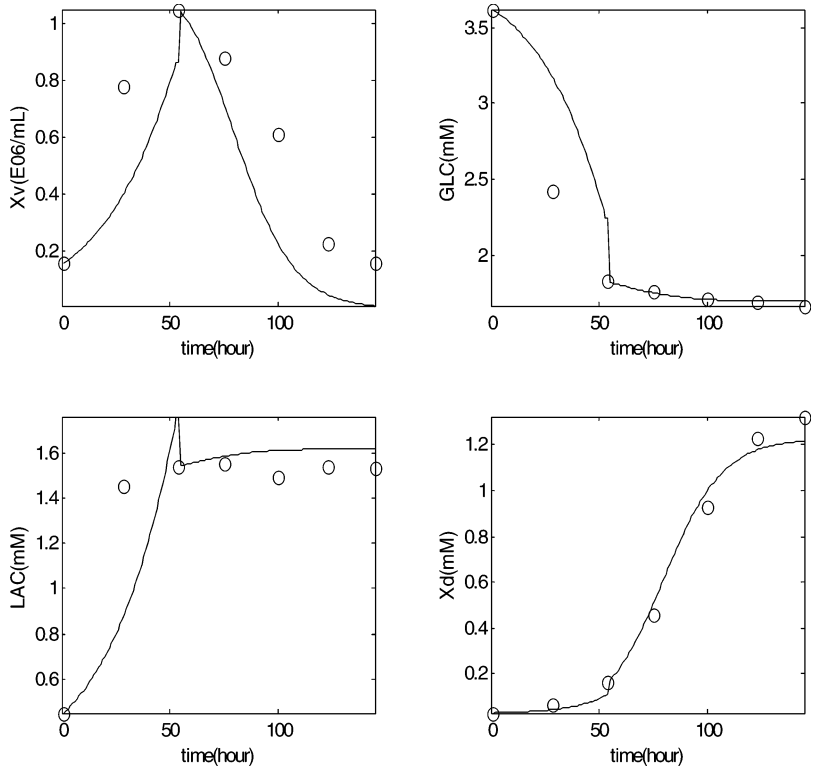

Figure 9. Comparison of model predictions (−) versus batch 2 of the testing data (○) (growth rate $\mu_2 = 0.0356\ h^{-1}$).

between the batches. The two batches shown in this paper correspond to the ones with the highest and lowest growth rates, i.e., $\mu_1 = 0.042\ h^{-1}$ in Figures 7 and 8 and $\mu_2 = 0.0356\ h^{-1}$ in Figure 9, respectively. From an operational point of view, it is convenient and useful to express the substrate and product fluxes as the function of the specific growth rate, μ. In contrast to amino acid and product (MAb) assay, the specific growth rate can be rapidly determined with minimal time delay during cell culture. The prediction of amino acid use, in turn, allows an "on-line" application of the model in an industrial setting.

As shown in these figures, generally the model predictions (denoted by solid lines) are in good agreement with the experimental data for both batches (denoted by circles). For the batch in Figure 9 the amino acid concentrations are not available and therefore only viable cells, glucose, lactate, and dead cell concentrations are plotted.

Although the experimental conditions between the batches were very similar, the variability in the growth rates is accompanied by similar variability in metabolite concentrations and viability. Thus, an additional test of model accuracy is that differences in cell growth rate give rise to corresponding different metabolite concentrations in the different batches. By comparing Figures 9 and 7, it can be observed that the batch with the lowest growth rate shown in Figure 9 results as expected in a lower production of lactate and slower consumption of glucose as compared to the faster changes in these variables recorded during the batch with the higher growth rate shown in Figure 7. This implies that a higher rate of glycolysis provides additional energy to bring about higher cell-specific growth rate. Lactic acid is a well-known inhibitory metabolite of mammalian cells. Apparently, the maximum lactate concentrations of less than 2 mM had no adverse effect on the specific growth rate.

A peculiar feature of this cell line is the absolute requirement for aspartic acid (Asp) during the growth phase. The mathematical analysis of the amino acid fluxes confirmed this requirement. Aspartic acid is exhausted following glutamine exhaustion. It is unclear, however, whether aspartic acid serves as a partial replacement of glutamine for energy metabolism and if the exhaustion of either or both of these amino acids brings about the onset of cell death.

Conclusions

A modeling procedure that takes into account cell metabolism has been used for the prediction of nutrient and product concentrations. The major contribution of the work is that it links cell metabolism to the dynamic mass balances for extracellular metabolites. Staring with a complex metabolic network, significant intracellular fluxes were first identified using MFA. However, because of its large dimensionality, the model based on this MFA results was still too impractical for model-based control and optimization. Therefore, a model reduction step followed and kinetics was added to the stoichiometric model so that a dynamic model was obtained that was well-suited for the model-based applications. Only a few basic experiments, for example, batch studies, were required for the identification of the model.

The results have shown that this model provides good prediction of the cell culture during both the exponential phase and the post-exponential phase, where the effects of cell production and cell death are expressed as functions of key nutrients.

The key benefits of the proposed model are as follows:

(1) The model predicts the concentrations of the major energy sources: glucose and glutamine.

(2) The model predicts the concentrations of the key amino acids during the cell culture process. These amino acids are the ones that are used for energy generation besides protein synthesis. Thus, the model may be used as a soft sensor to estimate the amino acids concentrations and may be used to control the addition of key nutrients during fed-batch culture.

(3) The model predicts product formation, and this may be used in the future as part of the overall optimization strategy.

The major novelty of this paper is that it proposes a model identification method, which is generic and can be easily applied to obtain a dynamic model for other cells lines. It could also be applied to identify significant nutrients and to study the effect of specific intracellular fluxes on cell growth and cell death. The only input parameter to the model is specific growth rate, μ. Consequently, online adaptation based on on-line estimation of the growth rate could be considered for cases when the growth rate is time-varying.

Notation

$\mathbf{a}_{exp}$	max specific reaction rate, exponential phase, μmol/(10^6 cells·h)
a_i	max specific reaction rate, μmol/(10^6 cells·h)
$\mathbf{a}_g$	max specific reaction rate, growth, μmol/(10^6 cells·h)
$\mathbf{a}_m$	max specific reaction rate, maintenance, μmol/(10^6 cells·h)
$\mathbf{a}_{post-exp}$	max specific reaction rate, post-exponential phase, μmol/(10^6 cells·h)
$\mathbf{A}$	matrix of stoichiometric coefficients
CH	volumetric cell-hour, 10^6 cells·h
j_i	intracellular flux i, μmol/(10^6 cells·h)
k_d	specific growth rate during the post-exponential phase, h^{-1}
k_o	nonviable cell inhibition parameter, (10^6 cells/mL·h)$^{-1}$
k_{Pi}, k_{Qi}, k_{Si}, k_{Ui}	half-saturation constant, mmol/L
r_i	Monod kinetics reaction rate, μmol/(10^6 cells·h)
R_i	specific conversion rate for metabolite i, μmol/(10^6 cells·h)
$\mathbf{R}$	vector of specific conversion rate for all metabolites, μmol/(10^6 cells·h)
$\mathbf{R}_{\xi,exp}$	metabolite conversion rates, exponential phase, μmol/(10^6 cells·h)
$\mathbf{R}_{\xi,g}$	metabolite conversion rates, growth, μmol/(10^6 cells·h)
$\mathbf{R}_{\xi,m}$	metabolite conversion rates, maintenance, μmol/(10^6 cells·h)
$\mathbf{R}_{\xi,post-exp}$	metabolite conversion rates, post-exponential phase, μmol/(10^6 cells·h)
t	culture time, h
X	viable cell concn, 10^6 cells/mL
$\xi(t)$	metabolite concn, mmol/L
μ	specific growth rate, exponential phase, h^{-1}
ψ	vector of concn, based on culture volume, of all metabolites, μmol/L

References and Notes

(1) Bernard, O.; Bastin, G. Identification of reaction networks for bioprocesses: determination of a partially unknown pseudo-stoichiometric matrix. *Bioprocess Biosyst. Eng*. **2006**, *27*, 293−301.

(2) Bonarius, H. P. J.; Hatzimanikatis, V.; Meesters, K. P. H.; de Gooijer, C. D.; Schmid, G.; Tramper, J. Metabolic flux analysis of hybridoma cells in different culture media using mass balances. *Biotechnol. Bioeng.* **1995**, *50*, 299−318.

(3) Dutton, R. L.; Scharer, J. M.; Moo-Young, M. Descriptive parameter estimation in animal cell culture. *Cytotechnology* **1998**, *26*, 139−152.

(4) Follstad, B. D.; Balcarcel, R. R.; Stephanopoulos, G.; Wang, D. I. C. Metabolic flux analysis of hybridoma continuous culture steady state multiplicity. *Biotechnol. Bioeng.* **1999**, *63*, 675−683.

(5) Frame, K. K.; Hu, W.-S. Kinetic study of hybridoma cell growth in continuous culture. I. A model for non-producing cells. *Biotechnol. Bioeng*. **1991a**, *37*, 55−64.

(6) Frame, K. K.; Hu, W.-S. Kinetic study of hybridoma cell growth in continuous culture. II. Behavior of producers and comparison to nonproducers. *Biotechnol. Bioeng.* **1991b**, *38*, 1020−1028.

(7) Gambhir, A.; Korke, R.; Lee, J.; Fu, P.; Europa, A.; Hu, W.-S. Analysis of cellular metabolism cells at distinct physiological states. *J. Biosci. Bioeng.* **2003**, *95* (4), 317−327.

(8) Gombert, A. K.; Nielsen, J. Mathematical modeling of metabolism. *Curr. Opin. Biotechnol.* **2000**, *11*, 180−186.

(9) biological systems: a link between metabolic and macroscopic description. *Math. Biosci.* **2005**, *193*, 25−49.
(10) Haag, J. E.; Wouwer, A. V.; Remy, M. A general model of reaction kinetics in biological systems. *Bioprocess Biosyst. Eng.* **2005**, *27*, 303−309.
(11) Hardy, K.; Stark, J. Mathematical models of the balance between apoptosis and proliferation. *Apoptosis* **2002**, *7*, 373−381.
(12) Hulhoven, X.; Wouwer, A. V.; Bogaerts, P. On a systematic procedure for the predetermination of macroscopic reaction schemes. *Bioprocess Biosyst. Eng.* **2005**, *27*, 283−291.
(13) Portner, R.; Schafer, T. Modelling hybridoma cell growth and metabolism − a comparison of selected models and data. *J. Biotechnol.* **1996**, *49*, 119−135.
(14) Provost, A.; Bastin, G. Dynamic metabolic modeling under balanced growth condition. *J. Process Control* **2004**, *12*, 717−728.
(15) Provost, A.; Bastin, G. Agathos, S. N.; Schneider, Y.-J. Metabolic design of macroscopic bioreaction models: Application to Chinese Hamster Ovary cells. *Bioprocess Biosyst. Eng.* **2006**, 29, 349−366.
(16) Sidoli, F. R.; Mantalaris, A.; Asprey, S. P. Modelling of mammalian cells and cell culture processes. *Cytotechnology* **2004**, *44*, 27−46.
(17) Wouwer, A. V.; Bogaerts, P. Special issue on bioprocess modeling and control. *Bioprocess Biosyst. Eng.* **2005**, *27*, 281−282.

Received March 30, 2006. Accepted November 22, 2006.

BP060089Y